GEMM-I riboswitches from *Geobacter* sense the bacterial second messenger cyclic AMP-GMP

Colleen A. Kellenberger[a,1], Stephen C. Wilson[a,1], Scott F. Hickey[a], Tania L. Gonzalez[b], Yichi Su[a], Zachary F. Hallberg[a], Thomas F. Brewer[a], Anthony T. Iavarone[c], Hans K. Carlson[d], Yu-Fang Hsieh[a], and Ming C. Hammond[a,b,2]

[a]Department of Chemistry, [b]Department of Molecular and Cell Biology, [c]QB3/Chemistry Mass Spectrometry Facility, and [d]Energy Biosciences Institute, University of California, Berkeley, CA 94720

Edited by Gisela Storz, National Institutes of Health, Bethesda, MD, and approved February 23, 2015 (received for review October 7, 2014)

Cyclic dinucleotides are an expanding class of signaling molecules that control many aspects of bacterial physiology. A synthase for cyclic AMP-GMP (cAG, also referenced as 3′-5′, 3′-5′ cGAMP) called DncV is associated with hyperinfectivity of *Vibrio cholerae* but has not been found in many bacteria, raising questions about the prevalence and function of cAG signaling. We have discovered that the environmental bacterium *Geobacter sulfurreducens* produces cAG and uses a subset of GEMM-I class riboswitches (GEMM-Ib, Genes for the Environment, Membranes, and Motility) as specific receptors for cAG. GEMM-Ib riboswitches regulate genes associated with extracellular electron transfer; thus cAG signaling may control aspects of bacterial electrophysiology. These findings expand the role of cAG beyond organisms that harbor DncV and beyond pathogenesis to microbial geochemistry, which is important to environmental remediation and microbial fuel cell development. Finally, we have developed an RNA-based fluorescent biosensor for live-cell imaging of cAG. This selective, genetically encodable biosensor will be useful to probe the biochemistry and cell biology of cAG signaling in diverse bacteria.

cGAMP | cyclic dinucleotides | fluorescent biosensor | bacterial signaling | gene regulation

Cyclic dinucleotides are a structurally related class of second messengers that are produced as key intracellular signals triggering physiological changes in response to environmental stimuli (*SI Appendix*, Fig. S1). Cyclic di-GMP (cdiG) was first identified to be widespread in bacteria through the prevalence of GGDEF domain-containing proteins encoded in sequenced genomes and studied for its regulation of the critical transition from motile to sessile, biofilm-forming lifestyles (1, 2). Recently, two other cyclic dinucleotides, cyclic di-AMP (cdiA) and cAMP-GMP (cAG or 3′,3′-cGAMP; Fig. 1*A*), have been discovered in bacteria (7, 8). Furthermore, an isomer of cAG containing a noncanonical 2′-5′ phosphodiester linkage (2′,3′-cGAMP) has been found to be produced in response to cytosolic DNA in mammalian cells (9–12). The mammalian sensor STING is stimulated by both bacterial cyclic dinucleotides and 2′,3′-cGAMP to activate the innate immune response (13). In bacteria, however, specific recognition of each second messenger is necessary to deconvolute the signaling pathways.

Of the three bacterial cyclic dinucleotides, the least is known about the signal transduction pathways for cAG (Fig. 1*A*). So far, the only component that has been identified is the *Vibrio cholerae* cAG synthase, DncV, which has homology to the mammalian cGAS enzyme through its 2′,5′-oligoadenylate synthase (OAS1) domain (8), but few homologs are found encoded in other bacterial genomes. To our knowledge, no sensors or effectors that respond selectively to cAG have yet been reported, although the second messenger has been shown to affect chemotaxis and intestinal colonization of *V. cholerae* (8). In addition, it remains an open question how prevalent cAG signaling is in bacteria.

Previously, we developed an RNA-based fluorescent biosensor that could be used as a tool to visualize cdiG signaling in vivo (14). This biosensor was created by fusing a natural cdiG-sensing GEMM-I class riboswitch aptamer (Vc2) (15) to the Spinach aptamer (Fig. 1*B* and *SI Appendix*, Fig. S1 *B* and *C*) (16, 17). Although the WT Vc2 aptamer is highly selective for cdiG (15), we showed that engineering the binding pocket through a G20A mutation altered ligand selectivity to render the aptamer capable of binding cAG and cdiG with similar affinities (14). Intriguingly, prior phylogenetic analysis revealed that, whereas 76% of the sequences in the GEMM-I riboswitch class have a G at this position (referenced hereafter as G20, following the Vc2 numbering) (18) shown in crystal structures of the riboswitch-ligand complex to form a Hoogsteen base pair with cdiG (3, 4), 23% instead had an A20 that presumably allows for recognition of cAG. We thus surveyed several of these A20 phylogenetic variants through the fluorescent biosensor screen to determine if any GEMM-I sequences are naturally selective for cAG.

A screen of natural A20 GEMM-I sequences revealed that the majority display promiscuous binding to cAG and cdiG, similar to G20A Vc2-Spinach (*SI Appendix*, Fig. S2*A*). A few sequences retain cdiG selectivity or have undetermined selectivities. However, one initial candidate, Gm0970, demonstrated a marked selectivity for cAG (Fig. 1*C* and *SI Appendix*, Fig. S2*B*). This sequence is from the bacterium *Geobacter metallireducens* GS-15, which has 17 predicted GEMM-I riboswitches annotated in its genome (GenBank accession NC_007517.1). Analysis of all GEMM-I sequences from this species revealed that 15/17

Significance

Bacteria are hidden forces of nature. For example, *Geobacter* bacteria play important roles in geochemistry by reducing metals in the environment. Scientists also are exploring the application of these bacteria toward toxic metal remediation and as "living batteries" that can generate electricity from biowaste. However, there is limited understanding of the signaling pathways that regulate this extracellular metal-reducing activity. Here we have discovered that *Geobacter sulfurreducens* use riboswitch sensors for a signaling molecule called cAG to regulate this process, which is an unexpected finding because cAG was previously associated only with pathogenic bacteria. Furthermore, we have adapted the riboswitch to generate a fluorescent biosensor that can be used to visualize cAG signaling in live bacteria.

Author contributions: C.A.K., S.C.W., and M.C.H. designed research; C.A.K., S.C.W., S.F.H., T.L.G., Y.S., Z.F.H., T.F.B., A.T.I., H.K.C., and Y.-F.H. performed research; H.K.C. contributed new reagents/analytic tools; C.A.K., S.C.W., S.F.H., T.L.G., Y.S., Z.F.H., T.F.B., A.T.I., H.K.C., Y.-F.H., and M.C.H. analyzed data; and C.A.K. and M.C.H. wrote the paper.

The authors declare no conflict of interest.

This article is a PNAS Direct Submission.

Data deposition: The sequences reported in this paper are provided in *SI Appendix*. For a list of relevant GenBank accession numbers, see *SI Appendix*, Tables S2 and S3.

[1]C.A.K. and S.C.W. contributed equally to this work.

[2]To whom correspondence should be addressed. Email: mingch@berkeley.edu.

This article contains supporting information online at www.pnas.org/lookup/suppl/doi:10.1073/pnas.1419328112/-/DCSupplemental.

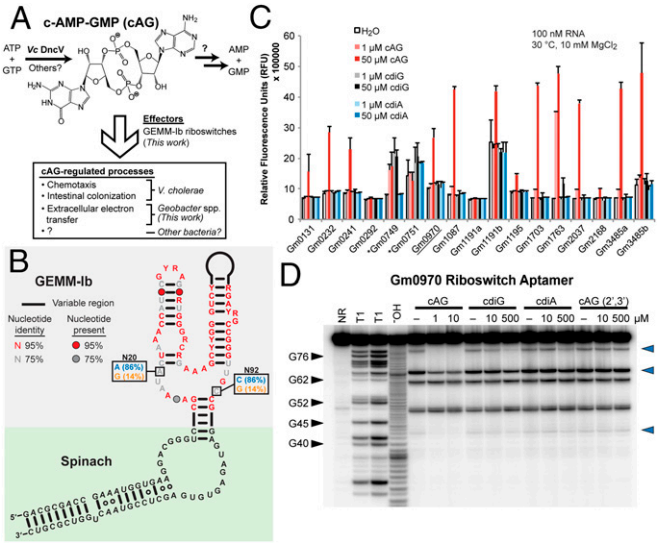

Fig. 1. GEMM-I riboswitches from *Geobacter* bacteria are selective for cAG. (*A*) Cyclic AMP-GMP signaling. (*B*) Sequence and secondary structure model of GEMM-I–Spinach fusion constructs based upon the crystal structures of the individual RNA components (3–6). The consensus for cAG-selective riboswitches in the GEMM-Ib subclass is shown. (*C*) Spinach-based selectivity screen of GEMM-I riboswitch aptamers from *G. metallireducens*. The initial candidate from the A20 screen is underlined (*SI Appendix*, Fig. S2). All sequences have an A20 except for those marked with an asterisk, which have a G20. (*D*) In-line probing analysis of cyclic dinucleotide selectivity for the Gm0970 riboswitch aptamer (also see *SI Appendix*, Fig. S4). No reaction (NR), treatment with RNase T1 (T1), which cleaves after G nucleotides, and partial base hydrolysis ($^{-}$OH) serve as control and ladders. Blue arrowheads indicate nucleotides that undergo conformational change in response to ligand binding.

contain an A20 and are selective for cAG or have undetermined selectivities (Fig. 1*C* and *SI Appendix*, Table S1). The remaining 2/17 contain a G20, and one binds both cAG and cdiG, whereas the other has undetermined selectivity. A similar screen of all GEMM-I sequences in *Geobacter sulfurreducens* Geobacter sulfurreducens strain PCA and select sequences in other *Geobacter* confirmed that the majority of GEMM-I sequences from *Geobacter* species preferentially bind cAG (*SI Appendix*, Fig. S3).

To validate that these riboswitch aptamers are naturally selective for cAG and that selectivity is not altered through the context of the Spinach aptamer, we performed an in-line probing analysis on the isolated Gm0970 and Gs1761 aptamers (Fig. 1*D* and *SI Appendix*, Figs. S4 and S5). Ligand-induced changes in the RNA fold are revealed by alteration of the in-line probing pattern, which corresponds to the extent of RNA self-cleavage at each nucleotide position. The Gm0970 aptamer has a dissociation constant (K_d) of ~16 nM for cAG and ~26 µM for cdiG, which means it is ~1,600-fold selective for cAG over cdiG. Similarly, the Gs1761 aptamer has a K_d of ~530 pM for cAG and ~660 nM for cdiG and thus is ~1,200-fold selective. Furthermore, high concentrations of up to 0.5 mM of cdiA or 2′,3′ cGAMP induced very little conformational change in either aptamer, indicating that the two riboswitch aptamers do not recognize these other cyclic dinucleotides. These data also demonstrate that natural GEMM-I riboswitches from *Geobacter* bind cAG selectively. To our knowledge, these RNAs are the first specific effectors for cAG that have been identified. These sequences constitute a previously unidentified subclass of GEMM-I riboswitches, herein termed GEMM-Ib, that respond selectively to cAG (Fig. 1*B*).

The cyclic dinucleotide content of *Geobacter* bacteria has not been analyzed previously, although bioinformatics analyses have predicted the presence of enzymes related to cdiG and cdiA signaling (19, 20) and corresponding GEMM-I and ydaO class riboswitches (15, 21). Our current results strongly suggest that these organisms also produce cAG as an endogenous signaling molecule, even though their genomes do not harbor any homologs of DncV. Thus, we performed organic-aqueous extraction of cyclic dinucleotides from *G. sulfurreducens* PCA cells. Liquid chromatography–mass spectrometry (LC-MS), MS/MS, and high-resolution mass spectrometry (HRMS) analysis revealed that all three bacterial cyclic dinucleotides are present in *G. sulfurreducens* cell extracts (Fig. 2 and *SI Appendix*, Figs. S6–S8). Only cdiG is observed when cells are grown to a similar density in media without supplemented yeast extract, and the corresponding analysis of 100% yeast extract did not yield any signal for cyclic dinucleotides (*SI Appendix*, Figs. S9 and S10). We detected a mass consistent with cAG in a miniscule amount only after analyzing concentrated HPLC fractions collected in the retention time range for cyclic dinucleotides (*SI Appendix*, Fig. S10). Thus, the amount of cAG isolated from the *G. sulfurreducens* cell extracts far exceeds the total amount that can be scavenged from the media, which implies that de novo synthesis of cAG is occurring. These experiments do not rule out a role for import mechanisms, but nevertheless demonstrate the presence of cAG as a native signaling molecule in *G. sulfurreducens*. Based on the ligand selectivity of their riboswitches, we expect cAG to be present in other *Geobacter* species as well. These results are significant because they provide, to our knowledge, the first evidence that cAG signaling extends to delta proteobacteria and, furthermore, beyond bacteria that harbor homologs of DncV.

We predict that the signaling molecule cAG turns on the expression of genes or operons associated with GEMM-Ib riboswitches via regulating the formation of rho-independent transcription terminators (*SI Appendix*, Tables S1 and S2). For example, the Gs1761 riboswitch upstream of the *pgcA* gene is expected to form a terminator stem with portions of the aptamer domain, but the terminator would be disrupted in the cAG-bound structure, as the P1 and P3 stems act as antiterminator sequences (Fig. 3*A*). In-line probing analysis of an extended riboswitch sequence in the presence of cAG reveals pattern changes consistent both with P1 and P3 stem formation and with disruption of the terminator stem (Fig. 3*B*). These structural changes are observed at low concentrations of cAG (starting at 10 nM), but are not observed with cdiG until concentrations are ~1,000-fold or greater (10–50 µM), which agrees with our previous results on selectivity for ligand binding. Thus, we demonstrate that cAG binding to the Gs1761 riboswitch aptamer disrupts terminator stem formation. Consistent with these results, an increase in full-length transcription with cAG was observed for another GEMM-Ib riboswitch (22).

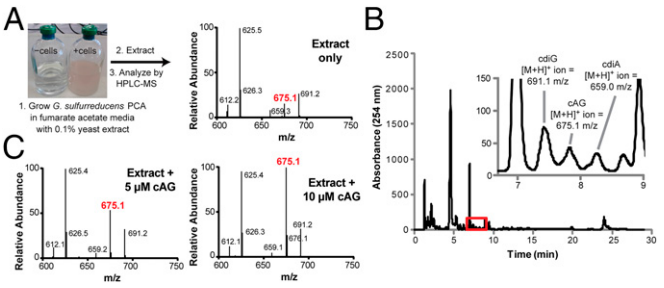

Fig. 2. *G. sulfurreducens* strain PCA produces cAG as well as cdiG and cdiA. (*A*) HPLC-MS analysis of *G. sulfurreducens* PCA cell extracts. Shown is the MS spectrum integrating the retention time region containing all three cyclic dinucleotides. (*B*) Full HPLC chromatogram of the cell extract. (*Inset*) The region containing peaks assigned to the cyclic dinucleotides (*SI Appendix*, Fig. S8*A*). (*C*) Similar analysis as shown in *A* for samples doped with 5 or 10 µM cAG.

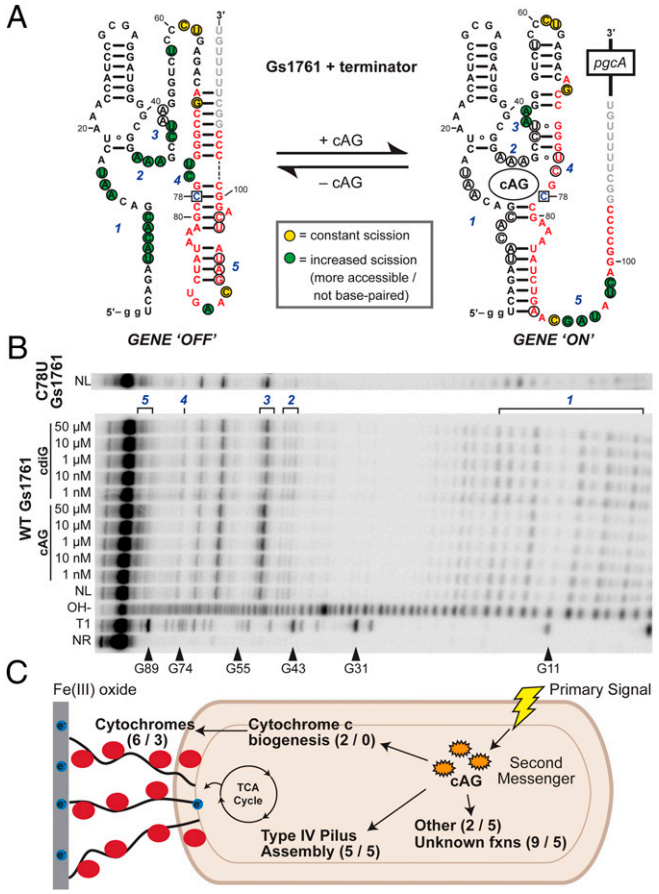

Fig. 3. GEMM-Ib riboswitches activate genes involved in extracellular electron transport in response to cAG. (*A* and *B*) In-line probing analysis of the full Gs1761 riboswitch (aptamer and transcription terminator) mapped onto the secondary structure models with and without cAG. Default transcription termination turns off gene expression, whereas cAG binding favors full-length transcription to the *pgcA*-coding sequence ("Gene ON"). Red nucleotides form the terminator stem. Gray nucleotides were excluded from the RNA construct tested. Blue numbers correspond to regions on the gel shown in *B*. The full gel for the C78U mutant is shown in *SI Appendix*, Fig. S11. (*C*) Schematic of extracellular electron transport that highlights the roles of genes turned on by cAG signaling. The number of genes are indicated for *G. sulfurreducens* and *G. metallireducens*, respectively (*SI Appendix*, Table S1). Depicted are cytochromes (red circles), pili (black lines), and electrons (blue circles).

A key metabolic feature of the *Geobacter* genus is the ability to perform extracellular electron transfer. In addition to playing an important role in natural geochemistry through the reduction of environmental metals (23), *Geobacter* have been described as "living batteries" that have the capacity to generate electricity from organic waste (24). Significantly, the genes regulated by GEMM-Ib class riboswitches and thus activated by cAG signaling include many that are functionally linked to this process (*SI Appendix*, Table S1). For example, the gene regulated by the Gs1761 riboswitch, *pgcA*, encodes a periplasmic cytochrome *c* protein that is conserved in *Geobacter* species and is more highly expressed during growth on insoluble Fe(III) oxide versus Fe(III) citrate (25, 26).

Interestingly, a C-to-T transition that maps to the Gs1761 riboswitch in the *pgcA* transcript was shown to double the rate of Fe(III) oxide reduction by *G. sulfurreducens* (27). We analyzed the extended C78U Gs1761 riboswitch sequence by in-line probing and found that the point mutation indeed destabilizes the terminator stem, as the observed pattern is similar to that of WT Gs1761 bound to cAG (Fig. 3*B*). However, unlike the WT riboswitch, the C78U mutant is insensitive to the presence of cAG or cdiG (*SI Appendix*, Fig. S11). This latter observation can be rationalized using the crystal structures of Vc2 bound to cdiG, which showed that the corresponding nucleotide forms a Watson–Crick base pair to the ligand (3, 4). Together, these results suggest that the C78U mutation to the riboswitch would constitutively turn on gene expression, which corroborates the ~15-fold increase of *pgcA* transcripts observed in the mutant strain (27). Taken together, our data provide functional evidence for cAG regulation via a GEMM-Ib riboswitch in vitro and explain the results of a prior study that implicated riboswitch-based regulation of the *pgcA* gene in vivo.

Several other cytochrome *c*-containing and biogenesis proteins appear to be regulated by cAG, including OmcS, which has been shown to be essential for metal oxide reduction and more highly expressed upon growth on insoluble Fe(III) or Mn(IV) oxides (28, 29). Although cytochrome genes are remarkably abundant in *Geobacter* species, they are not well conserved, making it difficult to base functional assignments of electron conduits on phylogenetic arguments (30). The identification of a subset of cytochromes coregulated by cAG suggests that they are part of a specific pathway and distinguishes them from others encoded in the genome.

In addition to extracellular cytochromes, *Geobacter* produce specialized type IV pili that are intimately involved in contacting insoluble metal sources, including electrodes, and there is evidence for direct electron shuttling by the pili (31), although this mechanism is still under active debate (32). The Gm0970 and Gs2033 riboswitches reside within an operon conserved in *Geobacter* that contains genes encoding minor pilins and pilus assembly proteins (*SI Appendix*, Fig. S12). Thus, the genes of known function associated with GEMM-Ib appear to be involved in extracellular electron transfer and allow us to propose a role for cAG signaling in the regulation of *Geobacter* electrophysiology (Fig. 3*C*). More significantly, the majority of genes associated with GEMM-Ib are of unknown or uncharacterized function, including two (Gsu2033 and Gsu2885) that are cotranscribed with PilMNOPQ and OmcAHG, respectively (*SI Appendix*, Fig. S12). An intriguing hypothesis is that these genes play a previously unrecognized role in extracellular electron transfer.

To further elucidate and study cAG-signaling pathways in *Geobacter* and other bacteria, we envisioned developing a genetically encodable fluorescent biosensor for live-cell imaging of cAG. The original Gm0970-Spinach construct, which harbors a 3-nt base-paired transducer stem (P1–3), displays modest (approximately twofold) fluorescence activation (Fig. 4*A*). Through optimization studies of the transducer stem that involved screening stems of different lengths (2–6 bp) and bulge deletions, two selective biosensors were developed that display much higher fluorescence activation (14.1-fold for P1–4 and 7.8-fold for P1–4delA) in response to cAG (Fig. 4*A* and *SI Appendix*, Fig. S13). Both biosensors exhibit similar apparent binding affinities in the low micromolar regime and binding kinetics for cAG at 3 mM Mg^{2+} and 37 °C (*SI Appendix*, Figs. S14 and S15). Importantly, fluorescence microscopy and flow cytometry experiments demonstrate that biosensors based on the Gm0970 riboswitch aptamer function in vivo (Fig. 4 *B* and *C* and *SI Appendix*, Figs. S16 and S17). Furthermore, these new fluorescent biosensors are able to clearly distinguish between enzymatic production of cAG versus cdiG.

It is clear that much remains to be discovered about cAG signaling. For example, whereas the cAG synthase DncV is found in *V. cholerae*, so far no phosphodiesterases or effectors for cAG have been identified in any organism. We now have revealed that cAG is produced by *G. sulfurreducens* and that *Geobacter* species harbor riboswitches as effectors that are selective for cAG. However, homology searches to DncV did not

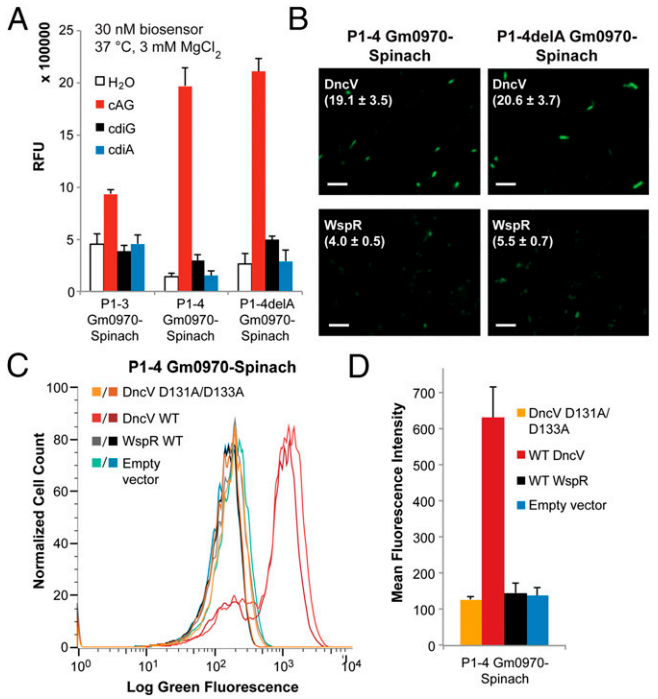

Fig. 4. A riboswitch-based fluorescent biosensor selectively detects cAG synthase activity. (*A*) Fluorescence activation and selectivity of Gm0970-Spinach biosensors with 100 μM ligands (also see *SI Appendix*, Fig. S13). (*B*) Fluorescence microscopy of *E. coli* coexpressing P1–4 and P1–4delA biosensors with a cAG (DncV) or cdiG (WspR) synthase. Mean fluorescence intensities with SEM are shown in parentheses (also see *SI Appendix*, Fig. S16). (Scale bars, 10 μm.) (*C*) Flow cytometry analysis of *E. coli* cells coexpressing the P1–4 Gm0970-Spinach biosensor and cyclic dinucleotide synthases or empty vector. (*D*) Quantitation of flow cytometry data for *E. coli* coexpressing a biosensor and synthase enzyme or empty vector. Error bars represent the SD in mean fluorescence of independent replicates of 20,000 cells analyzed.

identify any candidate cAG synthase in their genomes. The identification of novel enzymes and other signaling components that regulate the levels of cAG will be greatly assisted by the cAG-selective fluorescent biosensors that we have developed based on a GEMM-Ib riboswitch. These experiments are ongoing in our laboratory, and we expect will provide further insight into how widespread cAG signaling is in the eubacterial kingdom.

Another noteworthy aspect of cAG as a second messenger is its structural similarity to cdiG and cdiA. Although most *Geobacter* GEMM-I riboswitches that we tested were selective for cAG, a few were conspicuously promiscuous for cAG and cdiG (Fig. 1*C* and *SI Appendix*, Fig. S3). Furthermore, a limited survey of non-*Geobacter* sequences harboring the A20 variation demonstrated that most bind both cyclic dinucleotides (*SI Appendix*, Fig. S2*A*). Findings from this study lead to further intriguing questions regarding cyclic dinucleotide biology, including what is the molecular basis of selectivity versus promiscuity for different receptors and whether the hybrid nature of cAG promotes cross-activation of other cyclic dinucleotide-signaling pathways.

Materials and Methods

General Reagents and Oligonucleotides. GEMM-I–Spinach DNA oligonucleotides were purchased as Ultramers from Integrated DNA Technologies, and other oligonucleotides were purchased from Elim Biopharmaceuticals. Cyclic dinucleotides were purchased from Axxorra. 3,5-Difluoro-4-hydroxybenzylidene imidazolinone (DFHBI) was either purchased from Lucerna or was synthesized following previously described protocols (16) and was stored as an ~20 mM stock in DMSO. *G. sulfurreducens* PCA was obtained from the J. Coates laboratory at the University of California at Berkeley. Genomic DNA from *G. sulfurreducens* was isolated using the Purelink Genomic DNA mini kit (Invitrogen).

Bioinformatic Analysis of GEMM-I Variants. A Python-based program was developed to extract alignment and family data for a library of 1,991 putative GEMM-I riboswitches from the Rfam database (accession RF01051; rfam.xfam.org/) (33), calculate fold stabilization energies using RNAeval of the VIENNA software, and tabulate the data in an Excel spreadsheet as previously described (34). In particular, positions critical for cyclic dinucleotide binding were identified and analyzed for each sequence. In addition, the putative genes regulated by each riboswitch were elucidated by docking onto the GenBank website (www.ncbi.nlm.nih.gov/genbank/) and querying the organism's genome for genetic information using Biopython tools (35).

Removal of identical sequences from the alignment file left 1,347 unique GEMM-I sequences. Those from metagenomic sources were further omitted from analysis. A phylogenetic tree was generated from the remaining sequences using the PHYLIP software package (36). Briefly, evolutionary distances among the sequences were calculated using the F84 model, and a phylogenetic tree was constructed with the Neighbor-Joining/Unweighted Pair Group Method with Arithmetic Mean method. Sequences were selected using various criteria including, but not limited to: the presence of the A20 mutation, tractable P1 stems, evolutionary diversity, and interesting downstream genes.

In Vitro Transcription. Preparation of RNAs was carried out as previously described (14). Briefly, DNA templates for in vitro transcription were prepared via a PCR that added the T7 polymerase promoter sequence (*SI Appendix*, Tables S3 and S4). Templates were then transcribed using T7 RNA polymerase and were purified either by a 96-well spin column (ZR 96 Clean & Concentrator, Zymo Research) for screening experiments or by denaturing (7.5 M urea) 6% (wt/vol) PAGE for characterization experiments. RNAs purified by PAGE were subsequently eluted from gel pieces in Crush Soak buffer (10 mM Tris·HCl, pH 7.5, 200 mM NaCl, and 1 mM EDTA, pH 8.0), precipitated with ethanol, and resuspended in 1× TE buffer (10 mM Tris·HCl, pH 8.0, 1 mM EDTA). RNAs purified by a 96-well spin column were purified according to the manufacturer's protocol and were resuspended in 0.5× TE buffer. Accurate measurement of RNA concentration was determined after performing a hydrolysis assay to eliminate the hypochromic effect due to secondary structure in these RNAs (37).

In Vitro Fluorescence Assays of GEMM-I–Spinach Variants. To screen GEMM-I riboswitch aptamer selectivity, a solution of ligand (0, 1, 50, or 100 μM) and DFHBI (33 μM) was prepared in buffer containing 40 mM Hepes, 125 mM KCl, and 10 mM $MgCl_2$ at pH 7.5. Each RNA was renatured in buffer at 70 °C for 3 min and cooled to ambient temperature for 5 min before addition to the reaction solution at a final concentration of 100 nM. Binding reactions were incubated at 30 °C in a Corning Costar 3915 96-well black plate until equilibrium was reached (see activation curves in *SI Appendix*, Fig. S15). The fluorescence emission was measured using a Molecular Devices SpectraMax Paradigm plate reader with the following instrument parameters: 460 nm excitation and 500 nm emission. The background fluorescence of the buffer alone (without DFHBI) was subtracted from each sample to determine the relative fluorescence units.

To analyze the selectivity or binding affinity of RNA biosensor constructs, assays were run as described above, except at 37 °C with 3 mM $MgCl_2$ to mimic physiological conditions. Selectivity experiments were performed using 100 nM RNA and 100 μM ligand. Experiments to measure K_d were performed with 30 nM RNA and various ligand concentrations, and the fluorescence of the sample with DFHBI and RNA in buffer without ligand was subtracted to determine relative fluorescence units.

Biosensor Activation and Deactivation Assays. Activation and deactivation assays were performed as previously described (14). Briefly, to determine activation rate, the ligand (30 μM) and DFHBI (33 μM) in buffer were prepared and prewarmed to 37 °C. RNA (100 nM final concentration) was renatured in buffer at 70 °C for 3 min and then cooled to 37 °C before addition to the reaction solution. Immediately after the RNA was added, the fluorescence emission was measured every 2 min at 37 °C using the same plate-reader settings as for the ligand binding assays.

Deactivation assays were performed using buffer exchange to remove the cyclic dinucleotide ligand. RNA (100 nM) was mixed with ligand (30 μM) and DFHBI (33 μM) at 37 °C in a buffer containing 40 mM Hepes, 125 mM KCl, and 3 mM $MgCl_2$ at pH 7.5. Once the reaction had reached maximum fluorescence, half of the reaction was passed through an Illustra MicroSpin G-25 Column (GE Healthcare) that had been equilibrated with DFHBI (33 μM)

in buffer while the other half was passed through a column that had been equilibrated with ligand (30 μM), DFHBI (33 μM), and buffer. Immediately after elution of the RNA, the fluorescence emission was measured every 2 min at 37 °C using the same plate-reader settings as for the ligand binding assays.

In-Line Probing Assays. In vitro transcribed RNA was radiolabeled with γ-^{32}P ATP using T4 polynucleotide kinase (New England Biolabs) following standard procedures (38). After PAGE purification, RNAs were passed through an Illustra MicroSpin G-25 Column (GE Healthcare) and eluted with ddH_2O. In-line probing assays (1× in-line buffer: 50 mM Tris·HCl, pH 8.3, 20 mM $MgCl_2$, 100 mM KCl) were performed as previously described (37) for the extended Gs1761 riboswitch with terminator construct. The following modifications were made to the procedure to measure ligand-binding affinities below 1 nM for the Gm0970 and Gs1761 riboswitch aptamers. In-line reactions were prepared in 100 μL total volumes instead of the standard 10 μL. Thus, the final RNA concentration in each reaction was <<500 pM (this upper limit assumes 100% recovery from each purification step), which allowed us to determine subnanomolar dissociation constants. The reactions were quenched with 50 μL of 2× ULB (urea loading buffer, half of the standard volume), and 25 μL of the sample was loaded per lane onto a 10% urea–PAGE gel. To achieve ∼2,000–4,000 cpm per lane, the RNA had to be very efficiently radiolabeled (∼240,000–480,000 cpm/pmol). The no-reaction treatment with RNase T1 (T1), and partial base hydrolysis ($^-$OH) ladders were prepared as 10 μL reactions and quenched with 90 μL ddH_2O and 50 μL 2× ULB before loading 25 μL of each. Dried gels were exposed on a phosphorimager screen for several days and scanned using a Typhoon laser-scanning system (GE Healthcare).

Liquid Culture Growth of *G. sulfurreducens* PCA. From a glycerol stock, a 10 mL starter culture of *G. sulfurreducens* PCA in fumarate–acetate media alone or supplemented with 0.1% yeast extract was grown anaerobically at 30 °C for 5–7 d without shaking in anaerobic culture tubes sealed under nitrogen with 20 mm blue butyl rubber stoppers and aluminum crimps. Intermediate 50-mL cultures were inoculated at 1:10 dilution and then used to inoculate master 1 L cultures at 1:20 dilution in the same media. Cells were grown anaerobically in fumarate–acetate media with or without yeast extract at 30 °C until an OD_{600} of ∼0.4 was reached, which took about 2–3 d. Cells were harvested in 50 or 100 mL aliquots by centrifugation at 10,000 × *g* for 10 min at 4 °C, and pellets were stored at −80 °C.

The fumarate–acetate media contained the following in 1 L: 4 g sodium fumarate dibasic (25 mM sodium fumarate final concentration), 1.64 g sodium acetate (20 mM final concentration), 0.49 g $NaH_2PO_4{\cdot}2H_2O$, 0.97 Na_2HPO_4, 0.25 g NH_4Cl, 0.1 g KCl, 10 mL 100× vitamin mix (39), 1 mL 1,000× NB minerals mix (39), and 1.0 g yeast extract (Bacto brand, if used). The media was boiled and degassed by bubbling under nitrogen gas for 30 min while cooling, then aliquoted, sealed under anaerobic conditions, and autoclaved.

Liquid Culture Growth of *Escherichia coli* BL21 (DE3) Star. Fresh cultures of cells containing the pET31b GM0970 P1-4delA plasmid and dinucleotide cyclase enzymes in pCOLADuet-1 were inoculated from overnight starter cultures into 100 mL of LB/carb/kan media. Cells were grown aerobically to an OD_{600} of ∼0.5 and then induced with 1 mM isopropyl β-D-1-thiogalactopyranoside (IPTG) at 37 °C for 2 h. Cells were harvested by centrifugation at 10,000 × *g* for 10 min at 4 °C, and pellets were stored at −80 °C.

Cell Extraction from *G. sulfurreducens* PCA and *E. coli*. Cyclic dinucleotides were extracted as described previously (40) with the following modifications. A frozen cell pellet from 100 mL of liquid culture was thawed and resuspended in a 600 μL extraction buffer (40% methanol, 40% acetonitrile, 20% ddH_2O). The cell solution was incubated at 4 °C for 20 min and then at ambient temperature for 20 min. After centrifugation at 4 °C for 20 min at 13,200 × *g*, the supernatant was carefully removed and stored on ice. The remaining pellet was extracted twice more with 300 μL of extraction solvent as described. The combined supernatants were evaporated to dryness by rotary evaporation, and the dried material was resuspended in 250 μL ddH_2O. The extract was filtered through a 10-kDa MWCO Amicon Ultra-4 Protein Concentrator (Millipore) and used immediately or stored in aliquots at −20 °C.

Direct LC-MS Analysis of Cell Extracts. LC-MS analysis of *G. sulfurreducens* PCA cell extracts was performed using an Agilent 6120 Quadrupole LC-MS with an Agilent 1260 Infinity liquid chromatograph equipped with a diode array detector. Sample volumes of 20 μL were separated on a Poroshell 120 EC C18 column (50 mm length × 4.6 mm internal diameter, 2.7-μm particle size; Agilent) at a flow rate of 0.4 mL/min using a linear elution program of 0–10% solvent B over 20 min, where solvent A was H_2O + 0.05% TFA and solvent B was MeCN + 0.05% TFA. Under these conditions, the cyclic dinucleotides in extracts were found to elute always in the order of cdiG (7.3 ± 0.3 min), cAG (7.6 ± 0.3 min), and cdiA (7.9 ± 0.4 min), although there was variability in the retention times between runs. Thus, assignment of cyclic dinucleotide identity was made through analysis of the mass spectra.

Extract samples were analyzed by MS in the positive ion mode using the range of *m/z* = 600–800. When a broader range of 100–1,000 *m/z* was used, the expected mass for the corresponding cyclic dinucleotide was present, but was not the most abundant ion peak observed, even for the standards. This observation suggests that the relative ionization of cyclic dinucleotides is low under these conditions, and, furthermore, the cyclic dinucleotides may not be fully resolved from other small molecules present in the extract. Thus, the UV absorbance peaks detected at 254 nm may not be solely attributable to the cyclic dinucleotides.

HPLC Fractionation and MS Analysis (HRMS, MS/MS) of Cell Extracts. Discrete fractions from *G. sulfurreducens* PCA cell extracts were collected using an Agilent 1260 Infinity liquid chromatograph equipped with a diode array detector and analytical-scale fraction collector. Extract samples of 100–150 μL were separated on a Polaris C18-A column (250 mm length × 4.6 mm internal diameter, 5-μm particle size, 180-Å pore size; Agilent) at 50 °C with a flow rate of 1 mL/min. Solvent A was 100 mM ammonium acetate and solvent B was methanol. The elution program consisted of 0% B for 10 min, a linear gradient to 10% B over 1 min, isocratic conditions at 10% B for 4 min, a linear gradient to 30% B over 4 min, a linear gradient to 0% B over 1 min, and isocratic conditions at 0% B for 10 min. Eluted fractions were lyophilized multiple times to remove excess salts before mass spectrometry analysis.

HRMS and tandem mass spectrometry (MS/MS) measurements of collected fractions were performed using an Agilent 1200 liquid chromatograph (LC) that was connected in-line with an LTQ-Orbitrap-XL hybrid mass spectrometer equipped with an electrospray ionization source (Thermo Fisher Scientific). This instrumentation is located in the QB3/Chemistry Mass Spectrometry Facility at the University of California at Berkeley. The LC was equipped with a C18 analytical column (Viva C18: 150 mm length × 1.0 mm inner diameter, 5-μm particles; Restek) and a 100 μL sample loop. Solvent A was H_2O + 0.1% formic acid and solvent B was MeCN + 0.1% formic acid (vol/vol). The elution program consisted of isocratic conditions at 0% B for 3 min, a linear gradient to 35% B over 32 min, a linear gradient to 95% B over 0.1 min, isocratic conditions at 95% B for 4.9 min, a linear gradient to 0% B over 0.1 min, and isocratic conditions at 0% B for 19.9 min at a flow rate of 130 μL/min and 40 °C for the column compartment.

Full-scan mass spectra were acquired in the positive ion mode over the range of *m/z* = 100–1,000 using the Orbitrap mass analyzer, in profile format, with a resolution setting of 100,000 (at *m/z* = 400, measured at full width at half-maximum peak height). MS/MS spectra of selected precursor ions were acquired using collision-induced dissociation in the positive ion mode using the linear ion trap, in centroid format, with the following parameters: isolation width 3 *m/z* units, normalized collision energy 30%, activation time 30 ms, and activation Q 0.25. Data acquisition and analysis were performed using Xcalibur software (version 2.0.7 SP1, Thermo).

RNA Isolation and RT-PCR. RNA was extracted from *G. sulfurreducens* PCA cell pellets using the bacterial RNA purification protocol of the Universal RNA Purification Kit (CHIMERx) with lysozyme and RL buffer from the kit. Quality of total RNA was checked on a 1% agarose gel. RNA was treated with RQ1 DNase (Promega), and then 1 μg total RNA was used for cDNA synthesis in a 20 μL reaction using iScript Select cDNA Synthesis Kit (BioRad) or AMV Reverse Transcriptase (New England Biolabs) with random hexamer primers. RT-PCR was performed using primers designed to span intergenic regions (*SI Appendix*, Table S4) and Taq DNA polymerase (New England Biolabs).

Live-Cell Imaging by Fluorescence Microscopy and Flow Cytometry. Constructs for testing the Gm0970-Spinach biosensors in vivo were created as described previously (14, 16) by inserting the aptamers into a tRNA scaffold encoded within the pET31b plasmid (*SI Appendix*, Table S4). Biosensors and dinucleotide cyclase enzymes encoded in pET24a or pCOLA plasmids were coexpressed in *E. coli* BL21 (DE3) Star cells (Life Technologies). Fluorescence microscopy experiments and image analyses were carried out as described previously (14).

Preparation of cell samples for flow cytometry was carried out in a similar manner to the microscopy procedure. Briefly, after inoculating fresh LB/Carb/Kan cultures from overnight starter cultures, cells were grown to an OD_{600} of ~0.5 and then induced with 1 mM IPTG at 37 °C for 2 h. Cells were pelleted at room temperature for 4 min at 3,700 rcf, washed once with M9 minimal media at pH 7.0, and then resuspended in M9 minimal media containing 25 μM DFHBI to a final concentration of ~400 cells/μL based on OD_{600}. Cellular fluorescence was measured for 12,000–50,000 cells using either a BD Influx v7 cell sorter with BD FACS Sortware (Version 1.0.0.650) or a Guava easyCyte 8HT flow cytometer (Millipore) equipped with a 488-nm laser. The BD Influx v7 cell sorter is located in the Flow Cytometry Core Facilities at the University of California at Berkeley.

Additional data are available in *SI Appendix*.

ACKNOWLEDGMENTS. We thank John D. Coates and members of his laboratory for advice on experiments with *Geobacter*. This work was supported in part by NIH Grant DP2 OD008677 (to M.C.H.), a Department of Defense Science and Engineering Fellowship (to C.A.K.), a National Science Foundation graduate fellowship (to Z.F.H.), and NIH Training Grant T32 GM066698 (for Y.S. and T.F.B.). M.C.H. holds a Career Award at the Scientific Interface from the Burroughs Wellcome Fund.

1. Ross P, et al. (1987) Regulation of cellulose synthesis in Acetobacter xylinum by cyclic diguanylic acid. *Nature* 325(6101):279–281.
2. Römling U, Galperin MY, Gomelsky M (2013) Cyclic di-GMP: The first 25 years of a universal bacterial second messenger. *Microbiol Mol Biol Rev* 77(1):1–52.
3. Smith KD, et al. (2009) Structural basis of ligand binding by a c-di-GMP riboswitch. *Nat Struct Mol Biol* 16(12):1218–1223.
4. Kulshina N, Baird NJ, Ferré-D'Amaré AR (2009) Recognition of the bacterial second messenger cyclic diguanylate by its cognate riboswitch. *Nat Struct Mol Biol* 16(12):1212–1217.
5. Huang H, et al. (2014) A G-quadruplex-containing RNA activates fluorescence in a GFP-like fluorophore. *Nat Chem Biol* 10(8):686–691.
6. Warner KD, et al. (2014) Structural basis for activity of highly efficient RNA mimics of green fluorescent protein. *Nat Struct Mol Biol* 21(8):658–663.
7. Witte G, Hartung S, Büttner K, Hopfner K-P (2008) Structural biochemistry of a bacterial checkpoint protein reveals diadenylate cyclase activity regulated by DNA recombination intermediates. *Mol Cell* 30(2):167–178.
8. Davies BW, Bogard RW, Young TS, Mekalanos JJ (2012) Coordinated regulation of accessory genetic elements produces cyclic di-nucleotides for V. cholerae virulence. *Cell* 149(2):358–370.
9. Wu J, et al. (2013) Cyclic GMP-AMP is an endogenous second messenger in innate immune signaling by cytosolic DNA. *Science* 339(6121):826–830.
10. Gao P, et al. (2013) Cyclic [G(2′,5′)pA(3′,5′)p] is the metazoan second messenger produced by DNA-activated cyclic GMP-AMP synthase. *Cell* 153(5):1094–1107.
11. Ablasser A, et al. (2013) cGAS produces a 2′-5′-linked cyclic dinucleotide second messenger that activates STING. *Nature* 498(7454):380–384.
12. Diner EJ, et al. (2013) The innate immune DNA sensor cGAS produces a noncanonical cyclic dinucleotide that activates human STING. *Cell Reports* 3(5):1355–1361.
13. Danilchanka O, Mekalanos JJ (2013) Cyclic dinucleotides and the innate immune response. *Cell* 154(5):962–970.
14. Kellenberger CA, Wilson SC, Sales-Lee J, Hammond MC (2013) RNA-based fluorescent biosensors for live cell imaging of second messengers cyclic di-GMP and cyclic AMP-GMP. *J Am Chem Soc* 135(13):4906–4909.
15. Sudarsan N, et al. (2008) Riboswitches in eubacteria sense the second messenger cyclic di-GMP. *Science* 321(5887):411–413.
16. Paige JS, Wu KY, Jaffrey SR (2011) RNA mimics of green fluorescent protein. *Science* 333(6042):642–646.
17. Paige JS, Nguyen-Duc T, Song W, Jaffrey SR (2012) Fluorescence imaging of cellular metabolites with RNA. *Science* 335(6073):1194.
18. Smith KD, Lipchock SV, Livingston AL, Shanahan CA, Strobel SA (2010) Structural and biochemical determinants of ligand binding by the c-di-GMP riboswitch. *Biochemistry* 49(34):7351–7359.
19. Seshasayee ASN, Fraser GM, Luscombe NM (2010) Comparative genomics of cyclic-di-GMP signalling in bacteria: Post-translational regulation and catalytic activity. *Nucleic Acids Res* 38(18):5970–5981.
20. Bai Y, et al. (2012) Mycobacterium tuberculosis Rv3586 (DacA) is a diadenylate cyclase that converts ATP or ADP into c-di-AMP. *PLoS ONE* 7(4):e35206.
21. Nelson JW, et al. (2013) Riboswitches in eubacteria sense the second messenger c-di-AMP. *Nat Chem Biol* 9(12):834–839.
22. Nelson JW, et al. (2014) Control of exoelectrogenesis in Geobacter spp. by c-AMP-GMP, *Proc Natl Acad Sci USA* 112:5389–5394.
23. Lovley DR, Coates JD (1997) Bioremediation of metal contamination. *Curr Opin Biotechnol* 8(3):285–289.
24. Lovley DR (2008) The microbe electric: Conversion of organic matter to electricity. *Curr Opin Biotechnol* 19(6):564–571.
25. Ding Y-HR, et al. (2006) The proteome of dissimilatory metal-reducing microorganism Geobacter sulfurreducens under various growth conditions. *Biochim Biophys Acta* 1764(7):1198–1206.
26. Ding Y-HR, et al. (2008) Proteome of Geobacter sulfurreducens grown with Fe(III) oxide or Fe(III) citrate as the electron acceptor. *Biochim Biophys Acta* 1784(12):1935–1941.
27. Tremblay P, et al. (2011) A c-type cytochrome and a transcriptional regulator responsible for enhanced extracellular electron transfer in Geobacter sulfurreducens revealed by adaptive evolution. *Environ Microbiol* 13(1):13–23.
28. Mehta T, Coppi MV, Childers SE, Lovley DR (2005) Outer membrane c-type cytochromes required for Fe(III) and Mn(IV) oxide reduction in Geobacter sulfurreducens. *Appl Environ Microbiol* 71(12):8634–8641.
29. Aklujkar M, et al. (2013) Proteins involved in electron transfer to Fe(III) and Mn(IV) oxides by Geobacter sulfurreducens and Geobacter uraniireducens. *Microbiology* 159(Pt 3):515–535.
30. Butler JE, Young ND, Lovley DR (2010) Evolution of electron transfer out of the cell: Comparative genomics of six Geobacter genomes. *BMC Genomics* 11:40.
31. Vargas M, et al. (2013) Aromatic amino acids required for pili conductivity and long-range extracellular electron transport in Geobacter sulfurreducens. *MBio* 4(2):e00105–e00113.
32. Bonanni PS, Bradley DF, Schrott GD, Busalman JP (2013) Limitations for current production in Geobacter sulfurreducens biofilms. *ChemBusChem* 6(4):711–20.
33. Griffiths-Jones S, Bateman A, Marshall M, Khanna A, Eddy SR (2003) Rfam: An RNA family database. *Nucleic Acids Res* 31(1):439–441.
34. Karns K, et al. (2013) Microfluidic screening of electrophoretic mobility shifts elucidates riboswitch binding function. *J Am Chem Soc* 135(8):3136–3143.
35. Cock PJ, et al. (2009) Biopython: Freely available Python tools for computational molecular biology and bioinformatics. *Bioinformatics* 25(11):1422–3.
36. Felsenstein J (2005) PHYLIP (Phylogeny Inference Package) (Department of Genome Sciences, University of Washington, Seattle), Version 3.6.
37. Wilson SC, Cohen DT, Wang XC, Hammond MC (2014) A neutral pH thermal hydrolysis method for quantification of structured RNAs. *RNA* 20(7):1153–1160.
38. Regulski EE, Breaker RR (2008) In-line probing analysis of riboswitches. *Methods Mol Biol* 419:53–67.
39. Bruce RA, Achenbach LA, Coates JD (1999) Reduction of (per)chlorate by a novel organism isolated from paper mill waste. *Environ Microbiol* 1(4):319–329.
40. Spangler C, Böhm A, Jenal U, Seifert R, Kaever V (2010) A liquid chromatography-coupled tandem mass spectrometry method for quantitation of cyclic di-guanosine monophosphate. *J Microbiol Methods* 81(3):226–231.